Journal of Applied Fluid Mechanics, Vol. 11, No. 5, pp. 1239-1246, 2018.
Available online at www.jafmonline.net, ISSN 1735-3572, EISSN 1735-3645.
DOI: 10.29252/jafm.11.05.28522

Development of the Couple Stress Relationships for the Power Law Fluid and the Solution of Flow in Ceramic Tape Casting Process

F. Karami, A. Ahmadi Nadooshan† and Y. Tadi Beni

Engineering Faculty, Shahrekord University, Shahrekord, Iran

†*Corresponding Author Email: ahmadi@eng.sku.ac.ir*

(Received October 15, 2017; accepted April 6, 2018)

ABSTRACT

The absence of characteristic material length in the Navier-Stokes equations has led to the development of different couple stress theories. In the present study, for the first time, the relations of a couple stress theory are extended to power-law fluids. Moreover, considering the significance of the length scale in nano- and micromechanics, the relations of the extended theory were applied to Newtonian and power-law fluids in tape casting of ceramics. The obtained velocity was used to calculate the volumetric flow rate as well as the thickness of the ceramic tape. A comparison between the results of the Newtonian fluid and the analytical and experimental results indicated a close agreement between the present results and the results of other studies. Moreover, the tape thickness was obtained for different length scales (L) by numerically solving the velocity relations obtained for the non-Newtonian fluid. Also, the impact of casting speed on the tape thickness was shown for four power-law fluids assuming L=0.35.

Keywords: Couple stress tensor; Characteristic material length; Non-Newtoinian fluid; Tape thickness.

NOMENCLATURE

D_{ij}	symmetric part of the velocity gradient tensor	t	time
h_0	*the* height of the slurry channel	T_{ij}	force stress tensor
H	the height of the slurry in the reservoir	v	velocity
k	apparent viscosity	α	*the* correction factor for tape width accounting for side flow
K_i	mean curvature rate vector	β	*the* correction factor for weight loss aging of the tape
l	characteristic material length	δ	tape thickness
L	length scale	μ	Newtonian fluid viscosity
L_0	length of slurry channel	μ_{eff}	power law viscosity
M_{ij}	coupe stress tensor	ρ	density
n	power law exponent		
P	pressure		
Q	slurry flow rate		

1. INTRODUCTION

The concept of tensile forces applied to a volume element was first proposed by Cauchy (1829). He presented a continuum theory in which only central forces were used. This theory was later expanded by other scholars. Navier-Stokes equations in fluid mechanics were also developed ignoring the effect of couple stress. For instance, Stokes (1966) proposed the simplest generalization of the fluid mechanics by taking the couple stress into account. Basically, the problem with the Stokes theory is a large number of the unknown parameters in the equations which makes the theory hard to use. Unlike the case for larger scales, the classical theory fails to provide accurate solutions at small scales (i.e. nano- and microscale), where the presence of size and couple stresses become more effective. The reason is the lack of a characteristic material length, which has consequently led to the development of

different couple stress theories. The effects of size on physical and mechanical properties in small scale problems were explained by some experimental researches (Li *et al*. 2016; Zienert *et al*. 2010).

By showing the antisymmetric characteristic of the couple stress tensor and the relationship between volumetric couples and forces in solids, Hadjesfandiari and Dargush (2011) reduced the number of unknown components in couple stress equations. In another study (Hadjesfandiari and Dargush 2014), they investigated different generalized couple stress theories, including the original Cosserat theory (Cosserat 1909), Mindlin-Tiersten theory (Tiersten, 1962), Koiter couple stress theory (Koiter 1969), Yang modified couple stress theory (Yang *et al*. 2002) and strain gradient theories (Mindlin and Mindlin and Eshel (Mindlin 1965; Mindlin and Eshel 1968)), such as the micropolar, micro-Couette, and micromorphic theories, and discussed their degrees of freedom, excess deformations, and stated their incompatibilities. Li *et al*. (2014) used this theory to investigate a micro-tri-layer beam subject to electromagnetic torque. Micro-beams such as sensors, amplifiers, and activators are extensively applied in electromechanical systems.

Recently, Hajesfandiari *et al*. (2016) used this adaptable, size-dependent theory to investigate piezoelectric panels and proposed the relations of the boundary value problem as well as their integral forms for a two-dimensional specimen, implementing the size-dependent boundary value numerical method. They also addressed the interesting behavior of the size-dependent piezoelectric medium through a few numerical examples. Then, applying the same relations as the fluid equations, Hadjesfandiari *et al*. (2014) introduced a new couple stress theory which resolves the problems and incompatibilities of the Stokes couple stress theory. They extended the Newtonian fluid equations based on that theory and obtained an analytical solution for flow inside a straight pipe. Later, they used the theory to solve the lid-driven cavity flow (Hajesfandiari *et al*. 2015) inside a straight pipe.

The couple stress theories were applied in the study of lubrication, microfluidics, blood flow and multi-physics couplings. For example, numerous studies were conducted to investigate micropipes, microchannels and microshells applied in microfluidic devices based on the couple stress theories (Ansari *et al*. 2015; Zhou and Wang 2012). However, fluid flow in many of these problems does not follow Newtonian rheology such as biofluids (Chakraborty 2007) or polymer solutions (Bryce and Freeman 2010). Furthermore, the effectiveness of couple stresses on lubrication systems and non-Newtonian behavior of lubricants have been demonstrated in many researches (Jacobson 1991; Lin 1997; Ramanaiah and Sarkar 1979). Therefore, considering the different applications of non-Newtonian fluids, such as in biomechanics, lubrication, and electromechanical systems, the extension of couple stress theories to non-Newtonian fluids seems to be necessary. Tape casting is an economical method for mass production of thin ceramic films. These films are applied for substrates, also in electrical packages and as the dielectric in capacitors. The ceramic film thickness is around 100 μm , which is precisely specified and controlled. Therefore, many studies have been conducted aiming to determine the thickness of the ceramic film based on casting speed and flow rate. For example, Chou *et al*. (1987) calculated the behavior of a ceramic slurry during tape casting based on the principles of fluid dynamics. They managed to propose a relation for film thickness as a function of viscosity, pressure gradient, velocity, and the casting head geometry and modified the relation using experimental results. Pitchumani and Karbhari (1995) also studied the ceramic slurry as a non-Newtonian power-law fluid. They investigated the effect of the pressure gradient resulting from the height of the slurry in the casting head and the drag force resulting from movement on the bed by modeling the extended planar Couette flow and proposed an analytical relation for film thickness as a function of the slurry type and the geometrical and physical parameters involved in the process. Joshi *et al*. (2002) studied the power-law and the Bingham plastic flow in ceramic tape casting based on the classical theory and calculated the speed and the flow rate. Loest *et al*. (1994) addressed the numerical solution of the Bingham flow in tape casting and calculated the speed and flow rate using the finite element method (FEM), through which the thickness of the ceramic tape could be calculated.

In this paper, first, the relations of the couple stress theory are extended for the power-law fluids, after which they are used to solve the couple stress fluid flow in ceramic tape casting.

2. GOVERNING EQUATIONS

The continuity, and the linear and angular momentum equations are stated in indicial notation as follows based on the couple stress theory by Hajesfandiari *et al*. (2014):

$$\frac{D\rho}{Dt} + \rho v_{i,i} = 0 \tag{1}$$

$$\rho \frac{Dv_i}{Dt} = T_{ji,j} + \rho b_i \tag{2}$$

$$T_{[ji]} = -M_{[i,j]} \tag{3}$$

where the comma denotes differentiation with respect to the spatial (Eulerian) coordinates; ρ represents fluid density; v_i is the velocity components; $\frac{D}{Dt}$ denotes the material derivative; T_{ji} are the components of the force stress tensor; b_i represents the volumetric force components; M_i are the vector components of the couple stress

tensor, and the [ ] sign indicates the antisymmetric part of the tensor.

For an incompressible power-law fluid, the symmetric part of the force stress tensor is obtained from the following relation:

$$T_{(ji)} = -P\delta_{ij} + 2\mu_{\text{eff}} D_{ij} \tag{4}$$

$$D_{ij} = \frac{1}{2}\left(v_{i,j} + v_{j,i}\right) \tag{5}$$

$$\mu_{eff} = k\left(v_{i,j} + v_{j,i}\right)^{n-1} \tag{6}$$

where $T_{(ji)}$ represents the symmetric part of the force stress tensor, P shows the pressure, δ_{ij} is the Kronecker delta, and μ_{eff} is the viscosity of the power-law fluid. According to Eq. (3), a couple stress vector should also be defined for the antisymmetric part of the force stress tensor. Neglecting the changes in temperature and density, the couple stress vector for an incompressible fluid is expressed as follows:

$$M_i = -8\eta K_i \tag{7}$$

$$K_i = \frac{1}{4}\left(v_{k,ki} - v_{i,kk}\right) \tag{8}$$

K_i shows the curvature rate vector and η represents the second coefficient of viscosity that takes into account the effect of the length scale in the couple stress equations and is related to fluid viscosity:

$$\frac{\eta}{\mu} = l^2 \tag{9}$$

where l represents the material characteristic length which is not taken into account in classical fluid mechanics. It depends on the type of fluid and geometry, and can be calculated through either experimental methods or molecular dynamics simulation. Therefore, because of the existence of different effective conditions on molecular dynamics simulation, the results are represented for some arbitrary values of *l*. The second coefficient of viscosity (η) for the power-law fluid can be calculated from Eq. (6):

$$\eta = l^2 k\left(v_{i,j} + v_{j,i}\right)^{n-1} \tag{10}$$

$M_{i,j}$ can be found using Eqs. (7) and (8):

$$\begin{aligned} M_{i,j} = -2l^2 k\Big[&(n-1)\left(v_{i,j} + v_{j,i}\right)^{n-2} \\ &\left(v_{i,jj} + v_{j,ij}\right)\left(v_{k,ki} - v_{i,kk}\right) + \\ &\left(v_{i,j} + v_{j,i}\right)^{n-1}\left(v_{k,kij} - v_{i,kkj}\right)\Big] \end{aligned} \tag{11}$$

Therefore, the antisymmetric part of the force stress tensor is obtained according to Eq. (3):

$$\begin{aligned} T_{[ji]} &= -M_{[i,j]} = -\frac{1}{2}\left[M_{i,j} - M_{j,i}\right] \\ &= l^2 k\begin{bmatrix} (n-1)\left(v_{i,j} + v_{j,i}\right)^{n-2} \\ \left(v_{i,jj} + v_{j,ij}\right)\left(v_{k,ki} - v_{i,kk}\right) + \\ \left(v_{i,j} + v_{j,i}\right)^{n-1}\left(v_{k,kij} - v_{i,kkj}\right) \\ -(n-1)\left(v_{i,j} + v_{j,i}\right)^{n-2} \\ \left(v_{j,ii} + v_{i,ji}\right)\left(v_{k,kj} - v_{j,kk}\right) - \\ \left(v_{i,j} + v_{j,i}\right)^{n-1}\left(v_{k,kji} - v_{j,kki}\right) \end{bmatrix} \end{aligned} \tag{12}$$

The force stress tensor is obtained by combining symmetric and antisymmetric force stress tensors (Eqs. (4) and (12)):

$$T_{ji} = T_{(ji)} + T_{[ji]} \tag{13}$$

Therefore, the solution of the momentum equations will be possible with replacing of the obtained force stress tensor into the Eq. (2).

In what follows, these relations are used to solve the flow in ceramic tape casting. Applying this theory with considering the microscale thickness of the ceramic film, yield acceptable results.

3. FLOW GEOMETRY IN CERAMIC TAPE CASTING

Assume an incompressible steady flow in ceramic tape casting procedure as shown in Fig. 1. The flow geometry is solved assuming Newtonian and power-law fluids and based on the mentioned couple stress theory.

3.1 Newtonian fluid

Continuity and momentum equations for the steady, developed flow of a Newtonian fluid can be simplified according to the boundary conditions shown in Fig. 2:

$$v = 0 \tag{14}$$

Momentum along *y*-axis: $\frac{\partial P}{\partial y} = 0$ (15)

Momentum along x-axis:

$$\mu\frac{\partial^2 u}{\partial y^2} - \mu l^2\frac{\partial^4 u}{\partial y^4} = \frac{\mathrm{d}P}{\mathrm{d}x} \tag{16}$$

where u is the flow velocity along the *x*-axis which is only a function of *y*, and P denotes the pressure as a function of *x* according to Eqs. (15) and (16). The governing boundary conditions, according to Fig. 2, are as follows:

$$\text{at } y = 0 \qquad u = 0,\ M_x = 2\mu l^2\frac{\partial^2 u}{\partial y^2} = 0 \tag{17}$$

$$\text{at } y = h_0 \qquad u = u_c,\ M_x = 2\mu l^2\frac{\partial^2 u}{\partial y^2} = 0 \tag{18}$$

Therefore, the developed velocity profile can be calculated using Eqs. (16)-(18):

$$u(Y)=\frac{h_0^2}{\mu}\frac{\mathrm{d}P}{\mathrm{d}x}\left[L^2e^{\frac{Y}{L}}\frac{1-e^{-\frac{1}{L}}}{e^{-\frac{1}{L}}-e^{\frac{1}{L}}}+L^2e^{-\frac{Y}{L}}\frac{e^{\frac{1}{L}}-1}{e^{-\frac{1}{L}}-e^{\frac{1}{L}}}+\frac{1}{2}\left(Y^2-Y\right)+L^2\right]+u_cY \tag{19}$$

$$Y=\frac{y}{h_0},\ L=\frac{l}{h_0} \tag{20}$$

The flow rate of the casting process can be calculated by Eq. (19):

$$Q=\int_0^1 u(Y)h_0\mathrm{d}Y=\frac{h_0^3}{\mu}\frac{\mathrm{d}P}{\mathrm{d}x}\left[2L^3\frac{e^{\frac{1}{L}}+e^{-\frac{1}{L}}-2}{e^{-\frac{1}{L}}-e^{\frac{1}{L}}}-\frac{1}{12}+L^2\right]+\frac{u_ch_0}{2} \tag{21}$$

In Eq. (19), for $L=0$, the velocity profile is identical to that obtained from the classical theory:

$$u(Y)=\frac{h_0^2}{2\mu}\frac{\mathrm{d}P}{\mathrm{d}x}\left(Y^2-Y\right)+u_cY \tag{22}$$

This profile represents the velocity that is obtained by Navier-Stokes equations.

3.2 Power-law fluid

According to Eqs. (2), (4), and (12), the momentum equation for the steady-state, incompressible flow of power-law fluid along the *x*-axis is as follows:

$$\frac{\mathrm{dP}}{\mathrm{d}x}=\frac{\mathrm{d}}{\mathrm{d}y}\left[k\left(\frac{\partial u}{\partial y}\right)^{n-1}\left(\frac{\partial u}{\partial y}\right)\right]-kl^2\frac{\mathrm{d}}{\mathrm{d}y}\left[(n-1)\left(\frac{\partial u}{\partial y}\right)^{n-2}\left(\frac{\partial^2u}{\partial y^2}\right)^2+\frac{\partial^3u}{\partial y^3}\left(\frac{\partial u}{\partial y}\right)^{n-1}+\frac{\partial^3u}{\partial y^3}\left(\frac{\partial u}{\partial y}\right)^{n-1}\right] \tag{23}$$

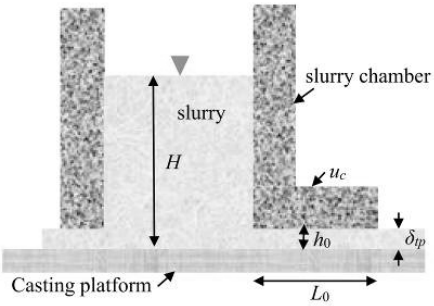

Fig. 1. Schematic diagram of the ceramic tape-casting process

Therefore, the velocity profile is calculated using the equation above and considering the boundary conditions from Eqs. (17), (18), and (20):

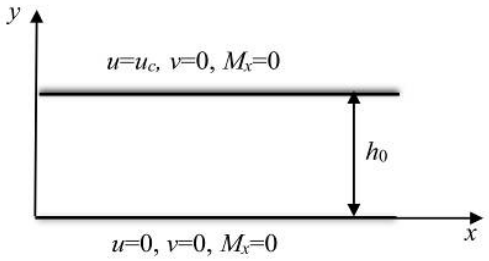

Fig. 2. Governing boundary conditions of flow in the ceramic tape-casting process

$$u(Y)=\int_0^Y\left\{\frac{h_0L}{k\sqrt{n}}\left(A_1e^{\sqrt{n}\frac{Y}{L}}-A_2e^{-\sqrt{n}\frac{Y}{L}}\right)+\frac{h_0}{k}\frac{\mathrm{d}P}{\mathrm{d}x}Y+\frac{A_3}{k}\right\}^{\frac{1}{n}}h_0\mathrm{d}Y \tag{24}$$

The constants A_1 and A_2 are obtained using boundary conditions:

$$A_1=\frac{\mathrm{d}P}{\mathrm{d}x}\left[\frac{1-e^{-\frac{\sqrt{n}}{L}}}{e^{-\frac{\sqrt{n}}{L}}-e^{\frac{\sqrt{n}}{L}}}\right] \tag{25}$$

$$A_2=\frac{\mathrm{d}P}{\mathrm{d}x}\left[\frac{e^{\frac{\sqrt{n}}{L}}-1}{e^{-\frac{\sqrt{n}}{L}}-e^{\frac{\sqrt{n}}{L}}}\right] \tag{26}$$

and the constant A_3 can be calculated from the following relation:

$$u_c=\int_0^1\left\{\frac{h_0L}{K\sqrt{n}}\left(A_1e^{\sqrt{n}\frac{Y}{L}}-A_2e^{-\sqrt{n}\frac{Y}{L}}\right)+\frac{h_0}{K}\frac{\mathrm{d}P}{\mathrm{d}x}Y+\frac{A_3}{K}\right\}^{\frac{1}{n}}h_0\mathrm{d}Y \tag{27}$$

4. RESULTS AND DISCUSSION

The results from two cases (Newtonian and power-law fluids) are discussed in this section. The velocity profile was plotted for the two cases and the diagram of ceramic film thickness with respect to casting speed was compared with previous studies at different length scales.

4.1 Newtonian fluid results

Figure 3 shows the non-dimensional velocity profile for various length scale values at $u_c=0$. The velocity profile for $L=0$ represents the classical solution. Here, $u_0=\left(h_0^2/2\mu\right)\left(\mathrm{d}P/\mathrm{d}x\right)$ and as expected, the velocity profile deviates from the classical solution as the size effect is increased. This shows the importance of using the non-classical theory at small scales. The value of $\mathrm{d}P/\mathrm{d}x$ for ceramic tape flow during casting is obtained as ρ_sgH/L_0.

Chou *et al.* (1987) evaluated their model for fluid flow in ceramic tape casting using experimental data.

The parameters considered in this evaluation are presented in Table 1. They proposed the following relation for estimation of the ceramic film thickness:

$$\delta_{tp} = \frac{\alpha\beta\rho_s Q}{\rho_{tp} u_c} \tag{28}$$

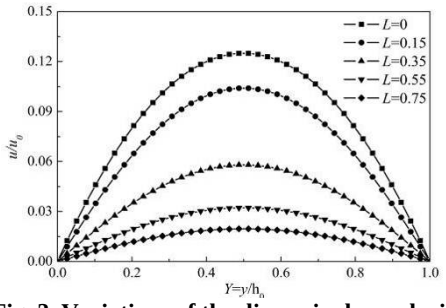

Fig. 3. Variations of the dimensionless velocity profile for various length scale value at $u_c = 0$

Joshi *et al.* (2002) used the same relation to estimate film thickness. In the present study, by calculating the flow rate from Eq. (21), the ceramic film thickness was obtained for the Newtonian fluid using Eq. (28) and was then compared to the analytical and experimental results from Chou *et al.* (1987) and Joshi *et al.* (2002) (Table 2). The results were represented for L=0.35 because of the best fitting with experimental results. The results suggest that the new theory gives an acceptable accuracy in comparison with the other models. Moreover, it is evident that film thickness is reduced as casting speed is increased and that the thickness considerably varies with speed at lower speeds, while the variations are mitigated as the speed is increased.

Table 1 Tape-casting process parameters for perovskite ceramic slurry (Chou *et al.* 1987)

Parameter	Value
η (Ns/m^2)	1.5
ρ_s (kg/m^3)	2030
ρ_{tp} (kg/m^3)	3440
α	0.89
h_0 (m)	0.402×10^{-3}
ΔP (Pa)	188
L_0 (m)	1.59×10^{-2}
β	0.6

4.2 Power-law fluid

Table 3 compares the ceramic film thickness for the non-Newtonian power-law fluid with the experimental results from Chou *et al.* (1987). The geometrical parameters from Table 1 were used in this investigation. As shown, the results from the couple stress theory for the non-Newtonian fluid are closer to the experimental results, showing more accuracy as compared to the case with a Newtonian fluid (Table 2). Figure 4 shows the velocity profile of the non-Newtonian fluid $n = 0.59$ at various length scales and for $u_c = 0.005\,\text{m/s}$. The parameters employed in this evaluation are presented in Table 4. The results were compared with those from the classical method ($L = 0$). As expected, the results deviate from the classical solution as the length scale is increased.

Pitchumani and Karbhari (1995) found the thickness of the film produced using a non-Newtonian power-law fluid by modeling a planar Couette flow. The variations of ceramic film thickness with casting speed for a power-law fluid with L=0 and n=0.59 are compared with the results from Pitchumani and Karbhari (1995) in Fig. 5. Furthermore, results are also presented for other length scales showing their impact. Clearly, as a result of the reduced speed and flow rate, the film thickness is reduced as the material characteristic length is increased. Furthermore, the film thickness changes much more with length scale at low velocities. As expected, the film thickness is reduced as casting speed is increased.

Figure 6 shows a diagram of film thickness with respect to casting speed (u_c) for different viscosity models (different powers) assuming an arbitrary length scale (L=0.35). It is clear from the figure that film thickness is considerably reduced as n is increased, showing the significance of the case with non-Newtonian fluid as compared to the Newtonian fluid. The geometrical parameters that are shown in either of Figs. 5 and 6 are extracted from Table 4.

The diagrams in Figs. 7-10 show the ceramic film thickness with respect to casting speed for different amounts of slurry height in the reservoir according to the geometrical parameters represented in Table 4. The changes in the thickness of the ceramic film in the case with the non-Newtonian power-law fluid are shown in Figs. 7, 8, 9, and 10 for L=0, 0.15, 0.35, and 0.55, respectively.

Table 2 Comparison of the present article results for L=0.35 and the analytical and experimental results

u_c (10^{-2}), m/s	δ_{tp} (10^{-6}), m			
	Present Model	Joshi's Model (Joshi *et al.* 2002)	Chou's Model (Chou *et al.* 1987)	Experimental Data (Chou *et al.* 1987)
1.277	63.84	64.4	64.4	66.0
1.621	63.73	64.2	64.2	63.5
2.059	63.65	64.0	64.0	63.5
2.988	63.55	63.8	63.8	63.5
4.396	63.48	63.6	63.6	62.2

It is evident from Fig. 7 that the film thickness is high at low speeds for all three slurry heights and only reducing as the speed is increased. The same behavior is also observed in Figs. 8-10. Moreover, all the diagrams in Figs. 7-10 indicate the film thickness to be increasing as the height of slurry in the reservoir, or in fact, the flow pressure gradient is increased. Comparing Figs. 7-10, it is concluded that the film thickness is reduced as the length scale is increased.

Table 3 Comparison of the present results for power-law fluid (n = 0.59 , L=0.35) and the experimental results

u_c (10^{-2}), m/s	δ_{tp} (10^{-6}), m	
	Present Model	Experimental Data (Chou *et al.* 1987)
1.277	64.74	66.0
1.621	64.40	63.5
2.059	64.10	63.5
2.988	63.76	63.5
4.396	63.45	62.2

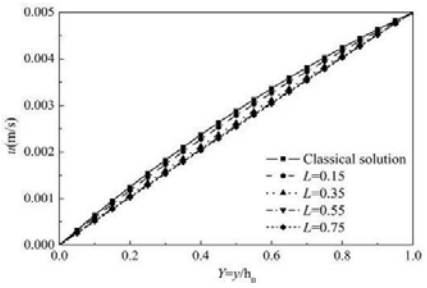

Fig. 4. Comparison of the velocity profile variations of power-law fluid for u_c = 0.005m/s , and various length scale values and classical solution

Table 4 Tape-casting process parameters for $BaTiO_3$ slurry (Pitchumani and Karbhari 1995)

Parameter	Value
$h_0(\mu m)$	100
$L_0(m)$	0.01
$\Delta P(Pa)$	981
ρ_s / ρ_{tp}	0.58
$K\ (Ns/m^2)$	2.7
α	0.89
β	0.60

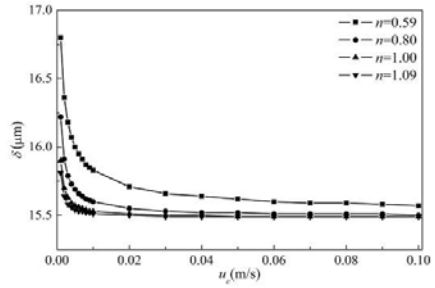

Fig. 5. Comparison of tape thickness variations against casting speed of power-law fluid(n=0.59) for various length scale values and Pitchumani and Karbhari (1995) results

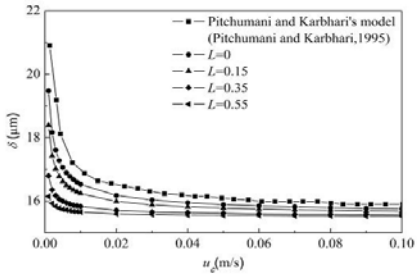

Fig. 6. Variations of tape thickness against casting speed for L=0.35, and different viscosity models

5. CONCLUSION

The non-Newtonian power-law fluid relations were extended to the couple stress theory by Hajesfaniari *et al.* (2014). These relations were used to study the flow in ceramic tape casting. A comparison between the velocity profiles of the classical and the non-classical theories shows the importance of the length scale which, when increased, leads to a greater difference between the results. Variations of the ceramic film thickness were obtained for different three power-law fluids based on the resulting casting speed (u_c). The results are different from those obtained from the classical theory and further deviate as the length scale is increased. Moreover, the film thickness was reduced in both specimens as the u_c and the length scale were increased. The difference between the results from the classical and the non-classical theories is reduced by increasing u_c. Examining the impact of the slurry height in the reservoir, it was found that the film thickness increases with the height of slurry at various length scales.

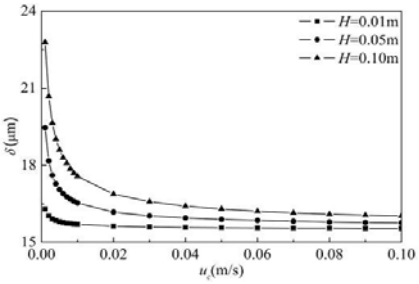

Fig. 7. Variations of tape thickness with casting velocity for various height values of the slurry in the reservoir (n=0.59 and L=0)

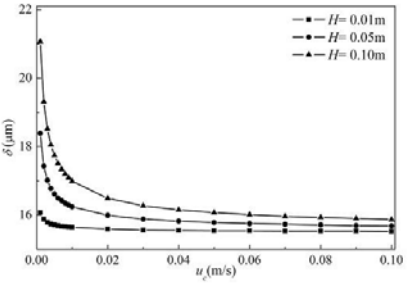

Fig. 8. Variations of tape thickness with casting velocity for various height values of the slurry in the reservoir (n=0.59 and L=0.15)

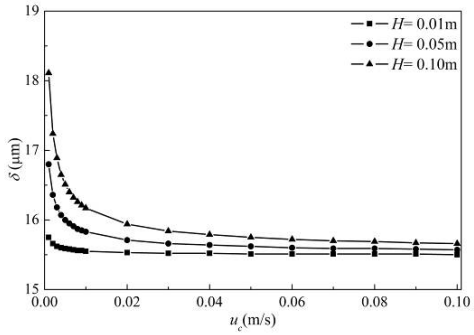

Fig. 9. Variations of tape thickness with casting velocity for various height values of the slurry in the reservoir (n=0.59 and L=0.35)

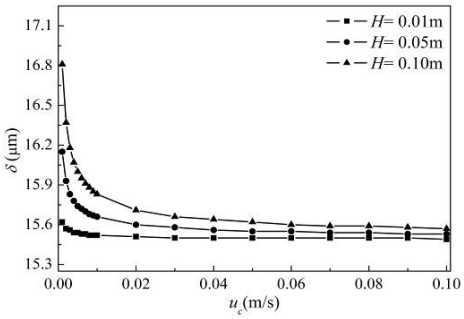

Fig. 10. Variations of tape thickness with casting velocity for various height values of the slurry in the reservoir (*n*=0.59 and *L*=0.55

REFERENCES

Ansari, R., R. Gholami, A. Norouzzadeh, and S. Sahmani (2015). Size-dependent vibration and instability of fluid-conveying functionally graded microshells based on the modified couple stress theory. *Microfluidics and Nanofluidics* 19, 509-522.

Bryce, R. M. and M. R. Freeman (2010). Extensional instability in electro-osmotic microflows of polymer solutions. *Physical Review E* 81, 036328.

Cauchy, A. L. (1829). Sur l'équilibre et le mouvement intérieur des corps considérés comme des masses continues. *Ex. de Math* 4, 293-319.

Chakraborty, S. (2007). Electroosmotically driven capillary transport of typical non-Newtonian biofluids in rectangular microchannels. *Analytica Chimica Acta* 605, 175-184.

Chou, Y. T., Y. T. Ko and M. F. Yan (1987). Fluid Flow Model for Ceramic Tape Casting. *Journal of the American Ceramic Society* 70, 280-282.

Cosserat, E. and F. Cosserat (1909). *Théorie des corps déformables (Theory of deformable bodies)*, A. Hermann et Fils, Paris, France.

Hadjesfandiari, A. R. and G. F. Dargush (2014). Evolution of generalized couple-stress continuum theories: a critical analysis. *arXiv preprint arXiv:1501.03112.*

Hadjesfandiari, A. R. and G. F. Dargush (2011). Couple stress theory for solids. *International Journal of Solids and Structures* 48, 2496-2510.

Hadjesfandiari, A. R., A. Hajesfandiari and G. F. Dargush (2014). Skew-symmetric couple-stress fluid mechanics. *Acta Mechanica* 226, 871-895.

Hajesfandiari, A., G. F. Dargush and A. R. Hadjesfandiari (2015). Size-dependent fluid dynamics with application to lid-driven cavity flow. *Journal of Non-Newton Fluid Mech* 223, 98-115.

Hajesfandiari, A., A.R. Hadjesfandiari and G. F. Dargush (2016). Boundary element formulation for plane problems in size-dependent piezoelectricity. *International Journal for Numerical Methods in Engineering* 108, 667-694.

Jacobson, B. O. (1991). *Tribology Series,* Chapter 5 Rheological models for non-Newtonian fluids, Elsevier 19, 53-68.

Joshi, S. C., Y. C. Lam, F. Y. C. Boey and A.I.Y. Tok (2002). Power law fluids and Bingham plastics flow models for ceramic tape casting. *Journal of Materials Processing Technology* 120, 215-225.

Koiter, W. T. (1969). couple-stresses in the theory of elasticity. *Philosophical transactions of the royal society of London* 867, 17-44.

Li, A., S. Zhou, , S. Zhou and B. Wang (2014). Size-dependent analysis of a three-layer microbeam including electromechanical coupling. *Composite Structures* 116, 120-127.

Li, L., Y. Hu, X. Li, and L. Ling (2016). Size-dependent effects on critical flow velocity of fluid-conveying microtubes via nonlocal strain gradient theory. *Microfluidics and Nanofluidics* 20, 76.

Lin, J. R. (1997). Effects of couple stresses on the lubrication of finite journal bearings. *Wear* 206, 171-178.

Loest, H., R. Lipp, and E. Mitsoulis (1994). Numerical Flow Simulation of Viscoplastic Slurries and Design Criteria for a Tape Casting Unit. *Journal of the American Ceramic Society* 77, 254-262.

Mindlin, R. D. (1965). Second gradient of strain and surface-tension in linear elasticity. *International Journal of Solids and Structures* 1, 417-438.

Mindlin, R. D. and N. N. Eshel (1968). On first strain-gradient theories in linear elasticity. *International Journal of Solids and Structures* 4, 109-124.

Pitchumani, R. and V. M. Karbhari (1995). Generalized Fluid Flow Model for Ceramic Tape Casting. *Journal of the American Ceramic Society* 78, 2497-2503.

Ramanaiah, G. and P. Sarkar (1979). Slider bearings lubricated by fluids with couple stress. *Wear* 52, 27-36.

Stokes, V. K. (1966). Couple stresses in fluids. *Physics of Fluids* 9, 1709–1715.

Tiersten, R. D. and H. F. Midlin (1962). Effects of couple-stresses in linear elasticity. *Archive for Rational Mechanics and Analysis* 11, 415-448.

Yang, F., A. C. M. Chong, D. C. C. Lam and P. Tong (2002). Couple stress based strain gradient theory for elasticity. *International Journal of Solids and Structures* 39, 2731-2743.

Zhou, X. and L. Wang (2012). Vibration and stability of micro-scale cylindrical shells conveying fluid based on modified couple stress theory. *Micro & Nano Letters* 7, 679-684.

Zienert, A., J. Schuster, R. Streiter and T. Gessner (2010). Transport in carbon nanotubes: Contact models and size effects. *physica status solidi (b)* 247, 3002-3005.